OPEN ACCESS

University of BRISTOL

Peer reviewed version

Link to published version (if available):
10.1021/acs.jpcb.9b01475

Link to publication record in Explore Bristol Research
PDF-document

University of Bristol - Explore Bristol Research
General rights

Following Bimolecular Excited State Proton Transfer Between Hydroxycoumarin and Imidazole Derivatives

Giordano Amoruso,[1] Victoria C. A. Taylor,[1,2] Marta Duchi,[1]
Emma Goodband[1] and Thomas A. A. Oliver[1,2,*]

[1] School of Chemistry, Cantock's Close, University of Bristol, Bristol, BS8 1TS, UK

[2] Bristol Centre for Functional Nanomaterials, School of Physics, University of Bristol, Bristol, BS8 1TH, UK

*Author for correspondence: tom.oliver@bristol.ac.uk

Abstract

The ultrafast dynamics of a bimolecular excited state proton transfer (ESPT) reaction between the photoacid 7-hydroxy-4-(trifluoromethyl)-1-coumarin (CouOH) and 1-methylimidazole (MI) base in aprotic chloroform-d_1 solution were investigated using ultrafast transient infrared (TRIR) and transient absorption (TA) spectroscopies. The excited state lifetime of the photoacid in solution is relatively short (52 ps) which at the millimolar photoacid and base concentrations used in our study precludes any diffusion-controlled bimolecular ESPT reactions. This allows the prompt ESPT reaction between hydrogen bonded CouOH and MI molecules to be studied in isolation, and the 'contact' ESPT dynamics to be unambiguously determined. Our time resolved studies reveal ultrafast ESPT from the CouOH moiety to hydrogen bonded MI molecules occurs within ~1 ps, tracked by unequivocal spectroscopic signatures of $CouO^-*$ photoproducts which are formed in tandem with HMI^+. Some of the ESPT photoproducts subsequently π-stack to form exciplexes on a ~35 ps timescale, minimizing the attractive Coulombic forces between the oppositely charged aromatic molecules. For the concentrations of CouOH and MI used in our study (up to 8 mM), we saw no evidence for excited state tautomerization of coumarin anions.

Introduction

Proton transfer is a fundamental reaction that is ubiquitous throughout biology and chemistry.[1] The transfer of a proton is the most facile method of delivering a positive charge. Yet, despite the apparent simplicity of a proton transfer,[2] it has enormous consequences for the outcome of chemical reactions, for example, catalyzing enzyme reactions,[3] or creation of trans-membrane proton gradients in photosynthesis that provide an essential driving force for ATP synthesis.[4,5]

In many cases, proton transfer is not instantaneous and requires stimulus to surmount the associated reaction barrier, which is often delivered via absorption of visible or ultraviolet light, however, the key reaction itself may occur on either ground[6] or excited[7] potential energy surface(s). The latter category of reaction is termed excited state proton transfer (ESPT), and the field has been dominated by the study of photoacids. Photoacids have larger acid dissociation constants in the excited state (pK_a*) compared to the ground electronic state, and these differences are frequently evaluated using the Förster cycle.[8,9] Recent studies have shown a strong correlation between photoacidity and the heteroatom–H stretching frequency of photoacids in a wide range of solvents.[10]

ESPT can be further categorized into two subclasses; (i) intramolecular ESPT where a proton is transferred between two heteroatoms on the same molecule[11,12] resulting in tautomerization[13–18]/isomerization,[19] or (ii) bimolecular ESPT where H$^+$ is transferred from the photoacid to a secondary molecule which may be part of the surrounding solvent,[20–23] a base solute molecule,[24–26] or a proximal protein residue.[27–30]

The timescale of ESPT depends greatly on the reaction subclass and underpinning mechanism, spanning the extremes of instantaneous/ballistic to diffusion limited.[31,32] Most reactions, however, sit in an intermediate regime where solvent re-organization must occur and/or proximal solvent molecules play a critical role in bridging or mediating ESPT.[33–35]

From a technical perspective, ESPT reactions are challenging both theoretically and experimentally, often necessitating an even-handed quantum mechanical treatment of both proton

and electrons using advanced theoretical methods,[36–38] and femtosecond temporal resolution to follow events that are commensurate to, or faster than, the solvent/environmental response.[39]

Chemical systems where the acid and base concentrations can be readily controlled and photoacidity manipulated via judicious chemical substitution provides one convenient approach to systematically explore the molecular mechanisms of ESPT. For example, functionalization of photoacids with electron withdrawing groups is known to reduce the pKa* via stabilization of the anion photoproduct.[40] In our study, we investigated an bimolecular ESPT reaction between two solute molecules: 7-hydroxy-4-(trifluoromethyl)-1-coumarin (CouOH) and 1-methylimidazole (MI), in the aprotic solvent chloroform-d$_1$ (CDCl$_3$)- see Scheme 1 for structures. The excited state acid–base reaction has previously been investigated in toluene solution by Westlake et $al.$ [25,26] using coherent Raman, time-correlated single photon counting, and transient absorption spectroscopies. In these studies, the excited state dynamics were only investigated for a select few CouOH:MI concentration ratios, where the MI base was always in excess. As part of their reaction scheme, Westlake et $al.$ reported ESPT between CouOH* and MI occurred a timescale of several tens of picoseconds and the coumarin anion photoproduct subsequently tautomerized on the excited state mediated by an excess of base MI molecules. We note that at the high concentrations used in the work by Westlake et $al.$, the probability for forming MI aggregates is significant.[41] Savarese et $al.$ also studied the CouOH–MI ESPT reaction using B3LYP density functional theory calculations.[42–44] Despite these prior studies, there are numerous open questions regarding the precise timescale of ESPT for this reaction due to the limited time resolution of prior studies, the definitive identification of the nascent photoproducts and their immediate fates.

In our study, we investigated the bimolecular ESPT reaction between CouOH and MI by systematically varying the concentration ratio between the photoacid and base to reveal unequivocal spectroscopic signatures of the photogenerated products and determine the involvement of any diffusion-assisted ESPT using a combination of transient absorption (TA) and time-resolved infrared (TRIR) ultrafast spectroscopies. This approach allowed us to gain insights into the earliest epoch of a prototypical biomimetic ESPT reaction and to track the fates of nascent photoproducts. Intentionally working at millimolar CouOH and MI concentrations made it possible to disentangle the photoproduct formation and rearrangement dynamics from the non-

radiative relaxation dynamics of 'free' CouOH molecules. Under these conditions, we exclude relaxation pathways such as bimolecular diffusion-assisted ESPT or coumarin anion tautomerization in chloroform solution. Our experimental findings are supported by density functional theory theoretical calculations.

Experimental and Theoretical Methods

7-hydroxy-4-(trifluoromethyl)-1-coumarin and 1-methylimidaziole were purchased from Sigma Aldrich and used without further purification. Deuterated chloroform ($CDCl_3$) solvent was used for all experiments (Sigma Aldrich, 99.8 atom % D, purity > 99.0%). Our studies explored a variety of different CouOH/MI solution mixtures.

TA and TRIR experiments were performed using an established ultrafast system.[45] Briefly, 330 nm pump laser pulses (~100 fs, 6 nm FWHM) was generated using a commercial optical parametric amplifier (OPA) and utilized in both TA and TRIR experiments. The pump fluence was attenuated to ~400 nJ at the sample. TA experiments used a white light supercontinuum probe, which was generated by focusing a small portion of the Ti:Sapphire fundamental into a rastered CaF_2 window. Pump scatter was removed using a 340 nm long pass filter. For TRIR measurements a second OPA was used to generate broadband (~150 fs, ~300 cm^{-1}) mid-IR probe pulses, centered at 1380 cm^{-1} or 1460 cm^{-1}. All ultrafast measurements were recorded using a magic angle polarization configuration. Samples were flowed continuously throughout experiments using a customized Harrick flow cell (CaF_2 windows), with 170 µm and 250 µm pathlengths for TA and TRIR measurements, respectively. Data were acquired at least three times for every mixture, using a freshly prepared solution each time.

Density functional theory (DFT) and time-dependent DFT (TD-DFT) theoretical calculations, with the ωB97XD exchange-correlation functional and a 6-31+G** basis set were used to optimize the minimum energy structures of various CouOH, MI and photoproduct structures in both ground and excited electronic states. Harmonic vibrational frequencies were calculated to verify the optimized structures obtained were true minima and to assist in the assignment of TRIR data. All calculations used a polarizable continuum model (PCM) to implicitly model the chloroform

solvent, and performed in the Gaussian09 computational suite.[46] An electron–hole density analysis was performed using Multiwfn.[47]

Steady state ultraviolet spectra were acquired using a Thermo Scientific Genesys 10S UV-Vis Spectrophotometer. Fourier-transform infrared (FTIR) data were acquired with a Perkin Elmer Spectrum Two FTIR Spectrometer. One and two-dimensional fluorescence spectra were collected with a Perkin-Elmer LS-45 Luminescence Spectrometer. All measurements were performed at room temperature (~20 $^{\circ}$C).

Results and Discussion

Ground State Association Equilibrium Characterization

We first investigated the ground state hydrogen bonding constant between CouOH and MI molecules in deuterated chloroform solution using linear ultraviolet absorption, FTIR and fluorescence spectroscopy.

The ultraviolet linear absorption spectra for several different CouOH/MI mixtures are displayed in Figure 1. It is important to note that MI absorbs at far shorter wavelengths (< 220 nm) than the displayed region. The absorption spectrum of 4 mM CouOH has a local maximum at 330 nm, which our TD-DFT calculations assign to a $\pi^*\leftarrow\pi$ electronic transition. The center of this band progressively red-shifts to 342 nm upon addition of up to 4 mM MI and the maximal absorbance increases. The observed red-shift of the absorption maximum matches previous measurements reported in toluene solution.[26] The similarity in absorption maxima of CouOH in toluene and chloroform solutions is unsurprising given the very similar dielectric constants and low associated polarities of both solvents. Ground state DFT calculations found that the only significantly favorable inter-molecular interactions between CouOH and MI moieties were hydrogen-bonding structures via the O–H⋯N bridge, which we henceforth refer to as CouOH⋯MI. Structures including π-stacking between the aromatic rings were found to be energetically unstable in S_0 and optimized to pseudo planar H–bonded structures. TD-DFT calculations show that the observed reduced transition energy associated with the $^1\pi\pi^*$ state of the coumarin molecule in the CouOH⋯MI complex mainly arises due to a stabilization of the CouOH π^* (LUMO), via a favorable H–bond between the CouOH hydroxyl group and the MI nitrogen lone pair. These

observations are similar to the red shifted absorption of the photoacid 1,3,6-trisdimenthylsulfonamide upon addition of hydrogen bonding acceptor molecules in aprotic chlorinated solvents.[48]

Figure 2 displays the FTIR spectra for CouOH, MI and various mixtures of CouOH and MI in CDCl$_3$ solution for part of the infrared fingerprint region. The major peaks in this region were assigned using DFT calculated vibrational frequencies (see Table 1). In CouOH/MI mixtures two additional vibrational peaks are present at 1331 cm^{-1} and 1526 cm^{-1}. We have assigned these bands using DFT calculated frequencies to coupled CouOH and MI vibrational modes.

The association constant between CouOH and MI molecules in CDCl$_3$ solution was determined by utilizing the aforementioned two features in the FTIR spectrum that are unique to the hydrogen bonded CouOH$\cdots$MI species. We solved the full second order equation[49] to calculate the equilibrium constant, without introducing any approximations as per Benesi-Hildebrand linearization.[50] Our analysis returned an association constant of 300 M^{-1} for reaction 1 in Scheme 1. The full details of our analysis are given in the supporting information (SI).

The value associated with the equilibrium constant has implications for our study: at the MI concentrations investigated (0.5–8 mM), there is a non-negligible percentage of free CouOH molecules in solution. For example, in equimolar solutions of 4 mM CouOH and MI, only ~41% of CouOH molecules are associated in the CouOH$\cdots$MI form. Thus, in our ultrafast spectroscopic studies, we expect that the dynamics of CouOH and CouOH$\cdots$MI will contribute to observed signals.

The fluorescence spectra of CouOH and mixtures of CouOH and MI in CDCl$_3$ solution are displayed in Figure 3. These data were acquired with 340 nm excitation, which coincides with the maximum absorption of CouOH in CDCl, with the 0.1 mM coumarin solution dominated by a single broad feature that peaks at ~405 nm. Full 2D fluorescence correlation spectra are given in Figure S3. Upon addition of MI, two additional features centered at 460 nm and 510 nm are present, and the intensities of these features is linearly proportional to the MI concentration, reminiscent of prior studies.[51] We assign these features to fluorescent photogenerated products

based on our time resolved studies (*vide infra*). 2D fluorescence spectra reveal that these new features are strongly correlated with the red-shifted absorbance (maximum at ~345 nm– see Figure S3) that is only present when MI is added to CouOH. With the equilibrium constant determined through FTIR measurements, we infer that the absorption cross-section for H-bonded CouOH/MI molecules is greater than of 'free' CouOH in $CDCl_3$ solution: in the linear absorption spectrum for the 1:1 mixture, we estimate that ~59% of CouOH molecules are 'free', and so 41% of hydrogen bonded CouOH molecules must be responsible for the large increase in absorption peaking at 345 nm. Along with the minor depletion of uncomplexed CouOH (evident at 310 nm), this can only be reconciled if the H-bonded species has a larger absorption cross-section than isolated CouOH.

The concentration of CouOH and MI used for fluorescence studies was far lower than for UV absorption or FTIR measurements, and we estimate that the hydrogen bonded CouOH$\cdots$MI species comprises no more than ~2% of the CouOH reservoir even for solutions containing the highest MI concentrations displayed in Figure 3. Despite isolated CouOH molecules being the dominant form of coumarin in chloroform solutions, the photoproduct emission bands are more intense than monomeric CouOH for solutions containing > 0.025 mM MI. This implies the fluorescence quantum yield of the photoproducts must be orders of magnitude higher than CouOH. At this stage, we can partly rationalize this observation based on the low fluorescence quantum yield of isolated CouOH, which we determined to be 5 ± 1 %. We also note that the relative intensity of the maxima at 460 nm and 510 nm are independent of concentration, which implies either that both bands arise from the same chemical species (*e.g.* a Franck-Condon vibronic progression), or alternatively if the bands correspond to different chemical photoproducts the relative product branching is independent of MI concentration.

Time Resolved Infrared Spectroscopy
TRIR studies were used to identify vibrational signatures of inter-molecular ESPT products between CouOH and MI in $CDCl_3$ solution. The data for 4 mM CouOH in $CDCl_3$ solution is displayed in Figure 4(a). Negative features in the TRIR data coincide with major features in the linear CouOH FTIR spectrum (see Figure 2) and correspond to loss of ground state CouOH parent molecules. The time-dependent intensity of these features reflects the percentage of molecules returned to S_0. Positive features arise from S_1 CouOH molecules or any photogenerated species.

The majority of vibrational features in the TRIR data were assigned using TD-DFT calculations–see Table 2.

Within the first 4 ps, the feature initially centered at 1393 cm^{-1} blueshifts by ~3 cm^{-1} to 1396 cm^{-1} accompanied by a slight increase in intensity. The 1396 cm^{-1} vibrational feature is associated with a ring breathing CouOH mode. DFT and TD-DFT calculated minimum energy geometries for S_0 and S_1, respectively, reveal that the structures vary by a slight expansion of the coumarin ring, and thus the ring breathing mode is intrinsically coupled to the $\pi^* \leftarrow \pi$ electronic transition. Initial Franck-Condon excitation of CouOH molecules into the S_1 state places molecules out-of-equilibrium with respect to the nuclear degrees of freedom associated with this vibration. Equilibration on the S_1 state leads to a change in the force constant associated with this vibrational mode, explaining the observed vibrational Stokes' shift. The kinetics of the positive transient at ~1445 cm^{-1} are the most spectrally isolated and thus used to determine the CouOH S_1 lifetime = 51.7 ± 4.2 ps (see Figure S10).

At the longest pump-probe time delay accessed in this study, the majority of both positive and negative features have almost fully decayed to zero signal intensity, however, the ground state bleach recovery is incomplete at $t = 1$ ns. A broad peak centered at 1490 cm^{-1} rises at $t > $ ~70 ps. DFT calculations were able to assign this vibrational feature to T_1 CouOH molecules which we assume will be relatively long-lived. At $t = 1$ ns, the bleach recovery is > 90% complete, and thus we infer that intersystem crossing in CouOH is a relatively minor non-radiative decay pathway. We rule out any fraction of molecules ring-opening via C–O bond cleavage on the pyran ring based on previous experiments of bare coumarin in acetonitrile,[52] and from our own ^{1}H-NMR experiments. 4 mM CouOH solutions were irradiated for up to five hours and then NMR data were acquired (Figure S2). These spectra did not contain any additional peaks associated with the build-up of ring-opened products.

Upon addition of 1 mM of MI to 4 mM CouOH solutions (Figure 4(b)) TRIR data contain three additional positive features centered at 1338, 1420 and 1466 cm^{-1}. The intensity of these bands increases further as the MI concentration is elevated to 8 mM (Figures 4(c,d)). These new transient

features are far longer lived (> 1 ns) than S_1 CouOH molecules in the absence of MI base (see Figure 4(a)).

Aside from these three new features in CouOH/MI mixtures, there is also a bleach feature present at 1515 cm^{-1} which corresponds to a MI vibration. Although MI does not absorb at 330 nm (the pump wavelength used in this study), the bleaching of this feature is instantaneous, meaning some portion of MI S_0 molecules are depopulated within the instrument response (TRIR ~300 fs, TA ~200 fs). We propose MI acts as a H$^+$ or H acceptor from photoexcited CouOH molecules, via ESPT (as previously reported[26]) or excited state H atom transfer, respectively.

To discriminate between these two possible photochemical reactions, we calculated a range of ground and excited state species corresponding to possible photogenerated products from intermolecular excited state proton transfer or H atom transfer (geometries of all the calculated structures are given in SI). The best agreement to the vibrational signatures in our experimental data was to the CouO$^-$*···HMI$^+$ ESPT products. Notably we found that vibrational bands mainly localized to the excited state anion had higher oscillator strengths than those associated with the protonated methyl-imidazole partner. Further, we note that the match is far poorer between experiment and theory for just CouO$^-$*, and thus the H–bond remains intact post-ESPT.

The electronic structure returned by TD-DFT calculations also support this picture; an exciton (electron-hole) analysis of the vertical excited state of CouOH*···MI and CouO$^-$*···HMI$^+$ products showed that electron and hole remain localized on the coumarin derivative after proton transfer, a finding which is only consistent with heterolytic bond fission (*e.g.* proton transfer) instead of formation of a radical pair via H atom transfer, which presumably would occur on a $^1\pi\sigma^*$ state.[53,54] Full details of the exciton analysis are given in the SI.

Further increasing the MI concentration, data shown in Figures 4(c) and (d), greatly enhances the intensity associated with the inter-molecular ESPT photoproduct features over the CouOH S_1 bands. All of the ESPT vibrational bands exhibit a time-dependent vibrational Stokes' shift of ~4–6 cm^{-1} within the first 20 ps towards higher frequencies. For the 1421 cm^{-1} feature, the peak maximum shifts to higher frequencies with a time constant of 9 ps (see analysis for 4 mM CouOH

and 8 mM MI solutions in Figure S11). This is far more dramatic than observed for S_1 CouOH ring breathing modes, and reconciled on the degree of molecular re-arrangement associated with $S_1 \leftarrow S_0$ excitation of neutral CouOH is small compared to the loss of a proton, anion formation and subsequent re-organization.

To elucidate the dynamics of excited state proton transfer, the kinetics of the spectrally isolated 1421 cm^{-1} CouO$^-$* transient became the focus of our quantitative analysis. We integrated over the whole peak area (1416–1425 cm^{-1}) to account for the observed shift in the peak wavenumber and growth in peak intensity and fit these data to a sum of exponentials. Analysis for two different CouOH/MI mixtures are displayed in Figure 5. For all datasets, the dynamics were fitted with a tri-exponential function (one rise and two decay components). Time constants returned from these analyses are tabulated for each CouOH/MI mixture in Table 4.

The kinetics returned from fitting are independent of MI concentration within the reported errors. We have determined the S_1 lifetime of CouOH to be 51.7 ± 4.2 ps which limits greatly reduces the probability of bimolecular diffusion controlled ESPT reactions between CouOH* and MI. We estimate that the upper limit for diffusion-controlled rate of reaction for our photoacid-base is 3.7×10^{10} M^{-1} s^{-1} (see SI for details and approximations). For the highest concentrations we examined (4 mM CouOH and 8 mM MI) this translates to a bimolecular reaction constant of 7.7 ns and greatly exceeds the excited state lifetime of the photoacid, precluding any diffusive ESPT. Resultantly all the ESPT products we observe originate from pre-hydrogen-bonded photoacid-base molecules. Therefore, increasing the MI concentration must only affect the amount of hydrogen-bonded S_0 CouOH$\cdots$MI molecules in solution prior to photoexcitation, and hence the ESPT product yield, but not the mechanism. We note that previous TRIR and time-resolved fluorescence studies have observed such diffusion controlled 'loose' ESPT dynamics for photoacids with longer excited state lifetimes and at orders of magnitude higher acid/base concentrations.[31,33,34,55]

Each time constant should be descriptive of a specific molecular process that occurs on the excited state: We assign the first time constant (~3 ps) to formation of CouO$^-$* photoproducts far from equilibrium, which as nuclei re-arrange to the new minimum energy structure, as evident from the

vibrational Stokes shift, leads to an increase in oscillator strength. Inevitably such processes greatly depend on the solvent re-organization timescale of chloroform, which is dominated by $\tau \sim 4$ ps.[56]

The inter-molecular ESPT products decay biexponentially with ~70 ps and > 1 ns time constants. Based on the TRIR data alone, it is not possible to assign mechanisms to the product decay pathways and requires insights from transient absorption spectroscopy.

Transient Absorption Spectroscopy

Transient absorption spectroscopy measurements provided further insights into the fates of ESPT products. A selection of these data for specific pump-probe time delays are shown in Figure 5, alongside the kinetics associated with specific probe wavelengths. Full datasets are provided in the supporting information (Figures S12–18).

The transient absorption data for 4 mM CouOH in CDCl$_3$ solution is displayed in Figure 6(a) for several representative pump-probe time delays. At early time delays ($t < 30$ ps) transient absorption signals are dominated by three main features: a negative signal centered at ~460 nm corresponding to a stimulated emission (SE) from S$_1$ CouOH molecules, and two positive signals peaking at 370 nm and 625 nm corresponding to S$_n \leftarrow$ S$_1$ excited state absorptions (ESAs). Direct comparison with the linear fluorescence spectrum (420 nm) reveals that the central frequency of the SE feature (460 nm) observed in TA experiments (Figure 6(a)) does not match the fluorescence maxima- see Figure 3. We reconcile this difference by requiring the oppositely signed ESA signal intensity is greater than the SE in the $\lambda < 420$ nm spectral region, and the negative feature present in the TA spectrum originates from the very the red edge of the SE.

At longer pump-probe time delays, ($t > 150$ ps) an additional positive feature centered at ~480 nm rises. On the basis of conclusions drawn from our TRIR data, we assign this to a CouOH T$_n \leftarrow$ T$_1$ ESA transient. The kinetics associated with the main S$_1$ CouOH ESA ($\lambda_{probe} = 370$ nm) and overlapping CouOH S$_1$ SE/T$_1$ ESA ($\lambda_{probe} = 460$ nm) are displayed in Figure 6(d).

Addition of 1 mM MI to 4 mM CouOH solutions dramatically changes the TA spectral profiles and associated kinetics (see Figures 6(b,e)); an additional ESA feature centered at ~400 nm

maximizes within the first ~100–150 ps, and the stimulated emission signal grows with intensity up to ~20 ps whilst simultaneously red-shifting by ~20 nm. The maximum of the red-shifted fluorescence (at $t > 20$ ps) matches the peak at 480 nm present in steady-state fluorescence data for CouOH···MI mixtures. The appearance of these new features and evolution within the first ~20 ps is rationalized in terms of excited state proton transfer reaction (*vide supra*).

When the concentration of MI is further increased (to a 1:2 CouOH:MI ratio) the TA spectra shown in Figure 6(c) are completely dominated by the ESA and SE signals we have attributed to inter-molecular ESPT products. Notably, the signal intensity compared to that of isolated CouOH (Figure 6(a)) is ~3 times as intense. A comparison of the kinetics for 402 nm and 480 nm probe wavelengths of the 4:1 and 1:2 CouOH:MI mixtures (Figures 6(e,f), respectively) show the associated dynamics are concentration dependent, but we recognize at these low absolute concentrations the majority of CouOH molecules are not hydrogen bound to a MI in the ground state prior to excitation, and thus the TA spectra represent a mixture of the dynamics of 'free' CouOH molecules, and the hydrogen bound CouOH···MI ESPT reaction.

To isolate the dynamics associated with inter-molecular excited state proton transfer, we subtracted the CouOH dataset (weighted) from mixture datasets. An example of this subtraction is given in the SI section (Figure S19). The kinetics (after subtraction) associated with integrating over the stimulated emission feature (between 460–500 nm) are shown in Figure 7 (a,b) for two CouOH/MI mixtures, corresponding to 1 mM and 8 mM MI added to 4 mM CouOH, respectively. These data were fit to a tri-exponential function, with two components accounting for an increased negative signal, and a one for the loss of stimulated emission. The time constants and amplitudes returned from these analyses for 6 different CouOH/MI mixtures are tabulated in Table 5.

Similar to our TRIR studies, the time constants returned by fitting are independent of MI concentration, and therefore physical phenomena underlying the dynamics must be related to the formation, rearrangement and subsequent relaxation of the CouO^{-*}···HMI$^+$ of ESPT photoproducts, once more indicating that absence of diffusion-controlled ESPT in our study.

The first time constant of ~1 ps is associated with a fast increase of stimulated emission from nascent CouO⁻* photoproducts, however, this is a shorter time constant than retrieved from TRIR studies. In the limit of the Born-Oppenheimer approximation, the change in electronic structure associated with transformation of CouOH* to CouO⁻* is seamless compared to the slow response of the nuclei. Therefore, the SE from CouO⁻* in TA measurements should be more sensitive to the ultrafast proton transfer reaction than the new transients observed in TRIR measurements and therefore we ascribe this fast time constant to the on-contact ESPT process. This observation agrees with the very small barrier to ESPT predicted by prior[43] and our own TD-DFT calculations (see General Discussion). The kinetics extracted from the TRIR data not only reflect population of photoproduct formation, but also a change in vibrational oscillator strength upon equilibration of the CouO⁻* products. The time-dependent Stokes' shift[57] observed in the TA data reflects the solvation dynamics associated with anion formation– see shifting minimum of SE band plotted in Figure S20.

There are some similarities with the work of Pines et al., who investigated the changes in hydrogen bonding network and ring geometry of a photoacid with a hydrogen bonding acceptor in the scenario where ESPT does not take place.[48] They observed a time-dependent red-shift in the SE signal, and attributed this to re-equilibration of the S_1 photoacid ring geometry and the hydrogen bonding bridge as influenced by the solvent re-organization timescale, but these data do not contain signals attributable to ESPT. As our spectral shifts in the CouOH/MI mixture solutions arise from the growth of coumarin anion photoproducts via ESPT, we are unable to comment on the changes along the H-bonding co-ordinate immediately prior or during ESPT."

The second time constant, ~33 ps, is associated with an increase in the SE signal and is also independent of MI concentration. One possible explanation for this observation is provided by our TD-DFT calculations which find a π-stacked exciplex of CouO⁻*···HMI⁺ is only 0.128 eV higher in energy than the minimum energy associated with the initial ESPT products. In this structure, the ∠OHN angle becomes ~120° and maintains the O⁻···H–N hydrogen bond, with the aromatic rings face-on and separated by ~3 Å. Whilst this is thermodynamically 'up-hill' for the specific calculated geometry, solvent fluctuations can easily provide the driving force for this re-arrangement. To form such species will require displacement of solvent molecules sandwiched

between the two rings, and thus partially explains the induction time, alongside any barrier that must be traversed. Such phenomena have been observed for neutral aromatic molecules that are hydrogen bonded in S_0, but π-stack in the S_1 state, *e.g.* benzene and derivatives,[58] as well as phenol.[59] Another characteristic of such process is a very strong $S_n \leftarrow S_1$ ESA signal,[59] as we observed for at $t > 30$ ps. The branching into this channel may be relatively minor, but the oscillator strength associated with exciplexes' ESA can be extraordinarily large, which for benzene dimer was estimated to be 76,000 M^{-1} cm^{-1}.[60] Our TD-DFT calculations for the minimum energy structure of the exciplex reveal that in the mid-infrared probe region we investigated, the exciplex vibrational frequencies are almost indistinguishable from the precursor initial ESPT products, but have ~3× smaller associated oscillator strengths. Therefore, we ascribe the ~13% decrease in TRIR signal on the order of tens of picoseconds to a transformation of the initial ESPT photoproducts into less IR active products, which manifests as a net loss in infrared signal intensity.

The third and final exponential component is as a result of photoproducts relaxation to the ground state, which occurs on timescales longer than 1 ns.

General Discussion

Using a combination of TRIR and TA spectroscopy and accompanying DFT calculations, we have elucidated the molecular mechanism of bimolecular excited state proton transfer dynamics between 7-hydroxy-4-(trifluoromethyl)-1-coumarin and 1-methylimidazole in chloroform solution, as schematically illustrated in Figure 8.

From our studies of CouOH solutions, we did not discern any solute-to-solvent ESPT, as $CDCl_3$ is a very poor proton acceptor. From our TRIR and TA studies, the S_1 excited state lifetime of CouOH was determined to be 51 ps, and we observed a minor intersystem crossing pathway (<10 %).

We determined the association constant for hydrogen bonding between CouOH and MI in $CDCl_3$ solution to be 300 M^{-1}. TRIR and TA studies of these solutions revealed direct spectroscopic signatures of inter-molecular ESPT between CouOH and MI, yielding CouO$^-$*$\cdots$HMI$^+$. TD-DFT one-dimensional scans along the intermolecular hydrogen-bonding co-

ordinate $R_{O—H\cdots N}$ are displayed in Figure 8(b) and show the minimum energy ESPT barrier is minimal (0.02 eV) at the TD-DFT/ωB97XD/6-31+G**/PCM level of theory. We note that despite the 1D nature of the PECs in Figure 8, the potential will be shallow in the Franck-Condon region, especially in the degrees of freedom surrounding the intermolecular hydrogen bond. Therefore not all molecules will experience the same barrier to ESPT, which in turn may be slightly higher for some of the ensemble.

At longer time delays, we infer that a portion of the initial CouO$^{-*}\cdots$HMI$^+$ products re-organize to form exciplexes (Figure 8(c)). Such products have very high ESA cross-sections, but whilst we do not know the quantum yield for the channel, we have been able to assign a rise time to this process.

Some of our findings are contrary to the prior study by Westlake et al.,[26] who examined ESPT between CouOH and MI in toluene solutions. They acquired TA data for two different concentrations of the photoacid and base: 1:5.9 and 1:14700 CouOH:MI ratios. These ratios are above those we studied (maximum of 1:2). We found that investigating the concentration dependence to TA data was crucial to deciphering whether any diffusional ESPT was important for 'free' CouOH molecules, in addition to the ESPT for hydrogen-bonded complexes, and isolation of the excited state reaction dynamics of uncomplexed CouOH. The reported kinetics in the prior study likely reflect a convolution of monomeric CouOH relaxation and ESPT, and may explain the discrepancy between our fitted returned time constants (1 ps and 30 ps) and the previously observed rise times of the SE (< 1 ps and ~5–10 ps). We also note that the prior work had a longer instrument response for TA measurements than our own (800 fs $vs.$ 200 fs) and are therefore unlikely to be able to resolve the < 1 ps rise time that we clearly observe. Westlake et al.[26] attributed the bimodal rise in SE to immediate H$^+$ transfer and delayed proton transfers, due to a sub-ensemble of molecules where the O–H$\cdots$N co-ordinate is not immediately in the correct configuration. Given the calculated minimum energy barrier to ESPT is so low, as per the calculations of Sarverse et al.[43], we rule out such a mechanism and assign the secondary rise component to exciplex formation.

Notably at the concentrations of MI used in our studies, we do not see evidence for any excited state tautomerization of Cou^{-*}, that previous experimental studies[26] and theory[43] have invoked to

explain a ~300 ps red shift in the fluorescence maxima for 0.34 mM CouOH and 500 mM MI solutions via time correlated single photon counting. The mechanism provided in these studies use a hydrogen bonded network of MI molecules around the Cou$^-$* to shuttle the proton from one end of the coumarin to the other, in a net tautomerization reaction. Such a mechanism is very reminiscent of gas phase cluster studies.[61] We anticipate that our TRIR studies would be very sensitive to this reaction, via changes in aromatic CouO*$^-$ vibrational frequencies, however, we do not see evidence for this process in either our TA or TRIR studies This may be due to the low concentrations we have focused on in our study, where such a multibody diffusion-controlled reaction is not accessible in our 1 ns probe window, or because the previously attributed mechanism is not operational.

Conclusions

We have investigated the bimolecular excited state proton transfer between 7-hydroxy-4-(trifluoromethyl)-1-coumarin and 1-methylimidazole in deuterated chloroform using ultrafast time-resolved infrared and transient absorption spectroscopies, accompanied by density functional theory calculations. In contrast to prior experimental studies, we have studied this system at low photoacid-base ratios to elucidate the molecular mechanism for ESPT and investigate whether there is a significant concentration dependence, *e.g.* diffusion-limited bimolecular ESPT, to the overall reaction. Through static infrared spectroscopy, we found that the equilibrium constant for hydrogen bonding between CouOH and MI is 300 M^{-1} in chloroform solution, and only molecules that are already in this configuration are primed for inter-molecular ESPT. Notably we do not see evidence for diffusion controlled ESPT as the CouOH S$_1$ lifetime is 52 ps, and the associated bimolecular time constant for reaction is 7.7 ns at the low absolute concentrations of acid and base investigated. This therefore permits us to investigate the 'contact' ESPT reaction of pre-hydrogen bonded photoacid-base molecules in isolation. With superior time resolution compared to prior studies of this photoacid-base pair,[26] we elucidate an ESPT time constant of ~1 ps. Time resolved infrared measurements reveal definitive vibrational signatures of CouO^{-*}$\cdots$HMI$^+$ ESPT photoproducts. Transient absorption measurements provide complimentary information on the fates of these initial ESPT products, which subsequently re-arrange to π-stack, thereby reducing the net charge on the overall complex. We do not see evidence for excited state tautomerization of the coumarin anion mediated via a chain of MI molecules. Either this is because our study focuses

on MI concentrations $\leq$ 8 mM and we are insensitive to any multibody reaction dynamics that occur on $\gg$ 1 ns timescales or no tautomeric species are formed in chloroform solutions. We envisage that our thorough and systematic study of CouOH and MI in CouOH solution will spur on high-level dynamical theoretical calculations to investigate the earliest epoch of a computationally tractable inter-molecular ESPT reaction.

Supporting Information

Supporting Information (SI) available: determination of ground state equilibrium constant; ^{1}H NMR spectroscopy of CouOH; full TRIR and TA datasets; DFT calculated minimum energy geometries of key chemical species used in the study; exciton analysis.

References

(1)   Eigen, M. Proton Transfer, Acid-Base Catalysis, and Enzymatic Hydrolysis. Part I: Elementary Processes. *Angew. Chemie Int. Ed. English* **1964**, *3*, 1–19.

(2)   Agmon, N. The Grotthuss Mechanism. *Chem. Phys. Lett.* **1995**, *50*, 456–462.

(3)   Kirby, A. J. Efficiency of Proton Transfer Catalysis in Models and Enzymes. *Acc. Chem. Res.* **1997**, *30*, 290–296.

(4)   Mitchell, P. Coupling of Phosphorilation to Electron and Hydrogen Transfer by a Chemi-Osmotic Type of Mechanism. *Nature* **1961**, *191*, 144–148.

(5)   Boyer, P. D. The ATP Synthase–a Splendid Molecular Machine. *Annu. Rev. Biochem.* **1997**, *66*, 717–749.

(6)   Warren, M. M.; Kaucikas, M.; Fitzpatrick, A.; Champion, P.; Timothy Sage, J.; Van Thor,

J. J. Ground-State Proton Transfer in the Photoswitching Reactions of the Fluorescent Protein Dronpa. *Nat. Commun.* **2013**, *4*, 1461–1468.

(7)   Nibbering, E. T. J.; Fidder, H.; Pines, E. Ultrafast Chemistry: Using Time-Resolved Vibrational Spectroscopy for Interrogation of Structural Dynamics. *Annu. Rev. Phys. Chem.* **2005**, *56*, 337–367.

(8)   Förster, T. Fluoreszenzspektrum Und Wasserstoffionen-Konzentration. *Naturwissenschaften* **1949**, *36* (6), 186–187.

(9)   Tolbert, L. M.; Solntsev, K. M. Excited-State Proton Transfer: From Constrained Systems to "Super" Photoacids to Superfast Proton Transfer. *Acc. Chem. Res.* **2002**, *35*, 19–27.

(10)   Psciuk, B. T.; Prémont-Schwarz, M.; Koeppe, B.; Keinan, S.; Xiao, D.; Nibbering, E. T. J.; Batista, V. S. Correlating Photoacidity to Hydrogen-Bond Structure by Using the Local O-H Stretching Probe in Hydrogen-Bonded Complexes of Aromatic Alcohols. *J. Phys. Chem. A* **2015**, *119*, 4800–4812.

(11)   Driscoll, E.; Sorenson, S.; Dawlaty, J. M. Ultrafast Intramolecular Electron and Proton Transfer in Bis(Imino)Isoindole Derivatives. *J. Phys. Chem. A* **2015**, *119* (22), 5618–5625.

(12)   Zhou, P.; Han, K. Unraveling the Detailed Mechanism of Excited-State Proton Transfer. *Acc. Chem. Res.* **2018**, *51*, 1681–1690.

(13)   Sengupta, P. K.; Kasha, M. Excited State Proton-Transfer Spectroscopy of 3-Hydroxyflavone and Quercetin. *Chem. Phys. Lett.* **1979**, *68*, 382–385.

(14)   Barbara, P. F.; Walsh, P. K.; Brus, L. E. Picosecond Kinetic and Vibrationally Resolved Spectroscopic Studies of Intramolecular Excited-State Hydrogen Atom Transfer. *J. Phys. Chem.* **1989**, *93*, 29–34.

(15)   Chapman, C. F.; Maroncelli, M. Excited-State Tautomerization of 7-Azaindole in Water. *J. Phys. Chem.* **1992**, *96*, 8430–8441.

(16)   Chudoba, C.; Riedle, E.; Pfeiffer, M.; Elsaesser, T. Vibrational Coherence in Ultrafast Excited State Proton Transfer. *Chem. Phys. Lett.* **1996**, *263*, 622–628.

(17)   Wu, Y. S.; Huang, H. C.; Shen, J. Y.; Tseng, H. W.; Ho, J. W.; Chen, Y. H.; Chou, P. T. Water-Catalyzed Excited-State Proton-Transfer Reactions in 7-Azaindole and Its Analogues. *J. Phys. Chem. B* **2015**, *119*, 2302–2309.

(18)   Park, S. Y.; Kim, H. B.; Yoo, B. K.; Jang, D. J. Direct Observation of Conformation-Dependent Pathways in the Excited-State Proton Transfer of 7-Hydroxyquinoline in Bulk

Alcohols. *J. Phys. Chem. B* **2012**, *116*, 14153–14158.

(19) Moriyama, M.; Kosuge, M.; Tobita, S.; Shizuka, H. Excited-State Intramolecular Proton Transfer Followed by Cis-Trans Isomerization of (1-Hydroxy-2-Naphthyl)-s-Triazine Derivatives. *Chem. Phys.* **2000**, *253*, 91–103.

(20) Takeuchi, S.; Tahara, T. The Answer to Concerted versus Step-Wise Controversy for the Double Proton Transfer Mechanism of 7-Azaindole Dimer in Solution. *Proc. Natl. Acad. Sci.* **2007**, *104*, 5285–5290.

(21) Pinto da Silva, L.; Simkovitch, R.; Huppert, D.; Esteves da Silva, J. C. G. Combined Experimental and Theoretical Study of the Photochemistry of 4- and 3-Hydroxycoumarin. *J. Photochem. Photobiol. A Chem.* **2017**, *338*, 23–36.

(22) Simkovitch, R.; Huppert, D. Photoprotolytic Processes of Umbelliferone and Proposed Function in Resistance to Fungal Infection. *J. Phys. Chem. B* **2015**, *119*, 14683–14696.

(23) Simkovitch, R.; Pinto da Silva, L.; Esteves da Silva, J. C. G.; Huppert, D. Comparison of the Photoprotolytic Processes of Three 7-Hydroxycoumarins. *J. Phys. Chem. B* **2016**, *120*, 10297–10310.

(24) Heo, W.; Uddin, N.; Park, J. W.; Rhee, Y. M.; Choi, C. H.; Joo, T. Coherent Intermolecular Proton Transfer in the Acid-Base Reaction of Excited State Pyranine. *Phys. Chem. Chem. Phys.* **2017**, *19*, 18243–18251.

(25) Westlake, B. C.; Brennaman, M. K.; Concepcion, J. J.; Paul, J. J.; Bettis, S. E.; Hampton, S. D.; Miller, S. A.; Lebedeva, N. V.; Forbes, M. D. E.; Moran, A. M.; et al. Concerted Electron-Proton Transfer in the Optical Excitation of Hydrogen-Bonded Dyes. *Proc. Natl. Acad. Sci.* **2011**, *108*, 8554–8558.

(26) Westlake, B. C.; Paul, J. J.; Bettis, S. E.; Hampton, S. D.; Mehl, B. P.; Meyer, T. J.; Papanikolas, J. M. Base-Induced Phototautomerization in 7-Hydroxy-4-(Tri-Fluoromethyl) Coumarin. *J. Phys. Chem. B* **2012**, *116*, 14886–14891.

(27) Chattoraj, M.; King, B. A.; Bublitz, G. U.; Boxer, S. G. Ultra-Fast Excited State Dynamics in Green Fluorescent Protein: Multiple States and Proton Transfer. *Proc. Natl. Acad. Sci.* **1996**, *93*, 8362–8367.

(28) Stoner-Ma, D.; Jaye, A. A.; Matousek, P.; Towrie, M.; Meech, S. R.; Tonge, P. J. Observation of Excited-State Proton Transfer in Green Fluorescent Protein Using Ultrafast Vibrational Spectroscopy. *J. Am. Chem. Soc.* **2005**, *127*, 2864–2865.

(29) Lill, M. A.; Helms, V. Proton Shuttle in Green Fluorescent Protein Studied by Dynamic Simulations. *Proc. Natl. Acad. Sci.* **2002**, *99*, 2778–2781.

(30) Carroll, E. C.; Song, S. H.; Kumauchi, M.; Van Stokkum, I. H. M.; Jailaubekov, A.; Hoff, W. D.; Larsen, D. S. Subpicosecond Excited-State Proton Transfer Preceding Isomerization during the Photorecovery of Photoactive Yellow Protein. *J. Phys. Chem. Lett.* **2010**, *1*, 2793–2799.

(31) Agmon, N.; Huppert, D.; Masad, A.; Pines, E. Excited-State Proton Transfer to Methanol-Water Mixtures. *J. Phys. Chem.* **1991**, *95*, 10407–10413.

(32) Pines, E.; Magnes, B. Z.; Lang, M. J.; Fleming, G. R. Direct Measurement of Intrinsic Proton Transfer Rates in Diffusion-Controlled Reactions. *Chem. Phys. Lett.* **1997**, *281*, 413–420.

(33) Mohammed, O. F.; Pines, D.; Pines, E.; Nibbering, E. T. J. Aqueous Bimolecular Proton Transfer in Acid-Base Neutralization. *Chem. Phys.* **2007**, *341*, 240–257.

(34) Rini, M.; Magnes, B. Z.; Pines, E.; Nibbering, E. T. J. Real-Time Observation of Bimodal Proton Transfer in Acid-Base Pairs in Water. *Science.* **2003**, *301*, 349–352.

(35) Agmon, N. Elementary Steps in Excited-State Proton Transfer. *J. Phys. Chem. A* **2005**, *109*, 13–35.

(36) Hynes, J. T.; Tran-Thi, T.-H.; Granucci, G. Intermolecular Photochemical Proton Transfer in Solution: New Insights and Perspectives. *J. Photochem. Photobiol. A Chem.* **2002**, *154*, 3–11.

(37) Hammes-Schiffer, S. When Electrons and Protons Get Excited. *Proc. Natl. Acad. Sci.* **2011**, *108*, 8531–8532.

(38) Hammes-Schiffer, S. Current Theoretical Challenges in Proton-Coupled Electron Transfer: Electron-Proton Nonadiabaticity, Proton Relays, and Ultrafast Dynamics. *J. Phys. Chem. Lett.* **2011**, *2*, 1410–1416.

(39) Simkovitch, R.; Shomer, S.; Gepshtein, R.; Huppert, D. How Fast Can a Proton-Transfer Reaction Be beyond the Solvent-Control Limit? *J. Phys. Chem. B* **2015**, *119*, 2253–2262.

(40) Prémont-Schwarz, M.; Barak, T.; Pines, D.; Nibbering, E. T. J.; Pines, E. Ultrafast Excited-State Proton-Transfer Reaction of 1-Naphthol-3,6-Disulfonate and Several 5-Substituted 1-Naphthol Derivatives. *J. Phys. Chem. B* **2013**, *117*, 4594–4603.

(41) Peral, F.; Gallego, E. Self-Association of Imidazole and Its Methyl Derivatives in Aqueous

Solution. A Study by Ultraviolet Spectroscopy. *J. Mol. Struct.* **1997**, *415*, 187–196.

(42)   Savarese, M.; Netti, P. A.; Adamo, C.; Rega, N.; Ciofini, I. Exploring the Metric of Excited State Proton Transfer Reactions. *J. Phys. Chem. B* **2013**, *117*, 16165–16173.

(43)   Savarese, M.; Netti, P. A.; Rega, N.; Adamo, C.; Ciofini, I. Intermolecular Proton Shuttling in Excited State Proton Transfer Reactions: Insights from Theory. *Phys. Chem. Chem. Phys.* **2014**, *16*, 8661–8666.

(44)   Raucci, U.; Savarese, M.; Adamo, C.; Ciofini, I.; Rega, N. Intrinsic and Dynamical Reaction Pathways of an Excited State Proton Transfer. *J. Phys. Chem. B* **2015**, *119*, 2650–2657.

(45)   Röttger, K.; Marroux, H. J. B.; Chemin, A. F. M.; Elsdon, E.; Oliver, T. A. A.; Street, S. T. G.; Henderson, A. S.; Galan, M. C.; Orr-Ewing, A. J.; Roberts, G. M. Is UV-Induced Electron-Driven Proton Transfer Active in a Chemically Modified A·T DNA Base Pair? *J. Phys. Chem. B* **2017**, *121*, 4448–4455.

(46)   Frisch, M. J.; Trucks, G. W.; Schlegel, H. B.; Scuseria, G. E.; Robb, M. A.; Cheeseman, J. R.; Scalmani, G.; Barone, V.; Petersson, G. A.; Nakatsuji, H.; et al. *Gaussian 09W, Revision D.01,* Gaussian Inc, Wallingford CT. 2016.

(47)   Lu, T.; Chen, F. Multiwfn: A Multifunctional Wavefunction Analyzer. *J. Comput. Chem.* **2012**, *33*, 580–592.

(48)   Pines, E.; Pines, D.; Ma, Y. Z.; Fleming, G. R. Femtosecond Pump-Probe Measurements of Solvation by Hydrogen-Bonding Interactions. *ChemPhysChem* **2004**, *5*, 1315–1327.

(49)   Thordarson, P. Determining Association Constants from Titration Experiments in Supramolecular Chemistry. *Chem. Soc. Rev.* **2011**, *40*, 1305–1323.

(50)   Concepcion, J. J.; Brennaman, M. K.; Deyton, J. R.; Lebedeva, N. V.; Forbes, M. D. E.; Papanikolas, J. M.; Meyer, T. J. Excited-State Quenching by Proton-Coupled Electron Transfer. *J. Am. Chem. Soc.* **2007**, *129*, 6968–6969.

(51)   Pines, D.; Pines, E.; Rettig, W. Dual Fluorescence and Excited-State Structural Relaxations in Donor-Acceptor Stilbenes. *J. Phys. Chem. A* **2003**, *107*, 236–242.

(52)   Murdock, D.; Ingle, R. A.; Sazanovich, I. V.; Clark, I. P.; Harabuchi, Y.; Taketsugu, T.; Maeda, S.; Orr-Ewing, A. J.; Ashfold, M. N. R. Contrasting Ring-Opening Propensities in UV-Excited α-Pyrone and Coumarin. *Phys. Chem. Chem. Phys.* **2016**, *18*, 2629–2638.

(53)   Mohammed, O. F.; Dreyer, J.; Magnes, B. Z.; Pines, E.; Nibbering, E. T. J. Solvent-Dependent Photoacidity State of Pyranine Monitored by Transient Mid-Infrared

Spectroscopy. *ChemPhysChem* **2005**, *6*, 625–636.

(54)   Sobolewski, A. L.; Domcke, W. Photoinduced Electron and Proton Transfer in Phenol and its Clusters with Water and Ammonia. *J. Phys. Chem. A* **2001**, *105*, 9275–9283.

(55)   Rini, M.; Pines, D.; Magnes, B. Z.; Pines, E.; Nibbering, E. T. J. Bimodal Proton Transfer in Acid-Base Reactions in Water. *J. Chem. Phys.* **2004**, *121*, 9593–9610.

(56)   Horng, M. L.; Gardecki, J. A.; Papazyan, A.; Maroncelli, M. Subpicosecond Measurements of Polar Solvation Dynamics: Coumarin 153 Revisited. *J. Phys. Chem.* **1995**, *99*, 17311–17337.

(57)   Stratt, R. M.; Maroncelli, M. Nonreactive Dynamics in Solution: The Emerging Molecular View of Solvation Dynamics and Vibrational Relaxation. *J. Phys. Chem.* **1996**, *100*, 12981–12996.

(58)   Miyasaka, H.; Masuhara, H.; Mataga, N. Picosecond Ultraviolet Multiphoton Laser Photolysis and Transient Absorption Spectroscopy of Liquid Benzenes. *J. Phys. Chem.* **1985**, *89*, 1631–1636.

(59)   Zhang, Y.; Oliver, T. A. A.; Ashfold, M. N. R.; Bradforth, S. E. Contrasting the Excited State Reaction Pathways of Phenol and Para-Methylthiophenol in the Gas and Liquid Phases. *Faraday Discuss.* **2012**, *157*, 141–163.

(60)   Cooper, R.; Thomas, J. K. Formation of Excited States in the Nanosecond-Pulse Radiolysis of Solutions of Benzene and Toluene. *J. Chem. Phys.* **1968**, *48*, 5097–5102.

(61)   Tanner, C.; Manca, C.; Leutwyler, S. Hydrogen-Bonded Ammonia Wire. *Science.* **2013**, *302*, 1736–1740.

Table 1. Experimentally observed and assigned calculated (DFT/ωB97XD/6-31+G**/PCM) ground state vibrational frequencies corresponding to the major peaks in Figure 2 and associated nuclear motions. All calculated frequencies were scaled by 0.96 to account for any anharmonicity.

Observed / cm^{-1}	Calculated / cm^{-1}	Assignment
		CouOH
1310	1305	Symmetric C–C phenol ring breathing/O–H bend
1347	1344	Anti-symmetric C–C phenol ring breathing/O–H bend
1407	1391	Out-of-phase C–C ring breathing on both pyrone and phenol moieties
1446	1442	In-phase C–C aromatic ring breathing mode on both pyrone and phenol ring /O–H bend
1518	1510	Symmetric C–C phenol ring breathing/C–O stretch
		MI
1421	1429	–CH$_3$ scissor
1505	1509	Anti-symmetric ring breathing
1518	1518	Symmetric ring breathing/N–CH$_3$ stretch
		CouOH···MI
1331	1352	Symmetric C–C phenol stretch/C–O stretch/MI ring breath
1526	1581	CouOH ring breathing/ CouOH O–H bend/MI ring breathing

Table 2. Experimentally observed and assigned calculated (TD-DFT/ωB97XD/6-31+G**/PCM) S_1 CouOH vibrational frequencies and associated nuclear motions. All calculated frequencies were scaled by 0.96 to account for any vibrational anharmonicity.

Observed / cm^{-1}	Calculated / cm^{-1}	Assignment
	CouOH (S_1)	
1316	1321	Anti-symmetric C–C phenol ring breathing/O–H bend
1396	1387	Symmetric C–C phenol ring breathing/anti-symmetric C–C stretch on pyrone
1449–1466	1420	In-phase C–C aromatic ring breathing mode on both pyrone and phenol ring
	1455	Anti-symmetric C–C phenol ring breathing
1525	1495	In-phase C–C aromatic ring breathing mode on both pyrone and phenol ring /O–H bend)
	CouOH (T_1)	
1449–1466	1429	Out-of-phase C–C ring breathing on both pyrone and phenol moieties
	1469	In-phase C–C ring breathing on both pyrone and phenol moieties
	1482	Out-of-phase C–C ring breathing on both pyrone and phenol moieties/C–O stretch on phenol ring

Table 3 TRIR experimental frequencies of the CouO$^-$*$\cdots$HMI$^+$ photoproducts, calculated (TD-DFT/ωB97XD/6-31+G**/PCM) excited state vibrational frequencies and associated nuclear motions. Calculated frequencies were scaled by 0.96 to account for any anharmonicity.

Observed / cm^{-1}	Calculated / cm^{-1}	Assignment
1338	1335	Out-of-phase C–C ring breathing on both pyrone and phenol moieties
1421	1370	In-phase C–C ring breathing on both pyrone and phenol moieties coupled to MI ring breathing
1466	1491	Symmetric C–C phenol ring breathing/in-phase C–O stretch coupled to N–H stretch

Table 4. Time constants and normalized amplitudes returned from fitting the 1420 cm^{-1} photoproduct band.

CouOH:MI / mM	τ_1 / ps	τ_2 / ps	τ_3 / ns	A_1	A_2	A_3
4:1	3.4 ± 0.4	66 ± 38	> 1	0.46	0.14	0.40
4:2	3.3 ± 0.2	72 ± 26	> 1	0.44	0.13	0.43
4:4	3.3 ± 0.2	70 ± 16	> 1	0.44	0.14	0.42
4:8	3.3 ± 0.2	71 ± 19	> 1	0.45	0.13	0.42

Table 5. Time constants and associated normalized amplitudes returned from tri-exponential fitting of SE band centered at 470 nm in TA data.

CouOH:MI / mM	τ_1 / ps	τ_2 / ps	τ_3 / ns	A_1	A_2	A_3
4:0.25	1.1 ± 0.3	35 ± 4.4	> 1	0.15	0.19	0.66
4:0.5	1.1 ± 0.2	34 ± 6.5	> 1	0.22	0.14	0.64
4:1	0.8 ± 0.1	30 ± 2.9	> 1	0.20	0.17	0.63
4:2	0.8 ± 0.2	27 ± 3.6	> 1	0.21	0.20	0.59
4:4	1.3 ± 0.2	41 ± 4.4	> 1	0.19	0.16	0.65
4:8	0.9 ± 0.1	28 ± 2.3	> 1	0.21	0.16	0.63
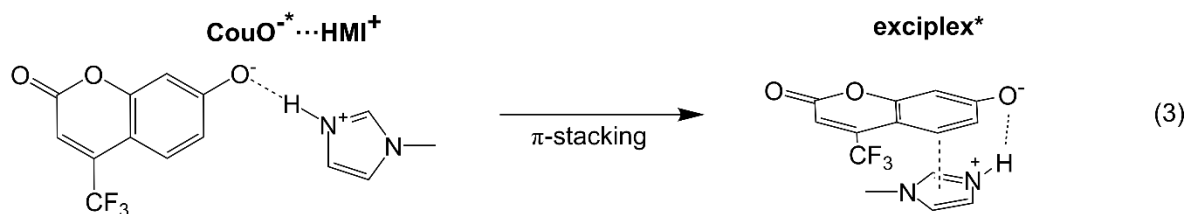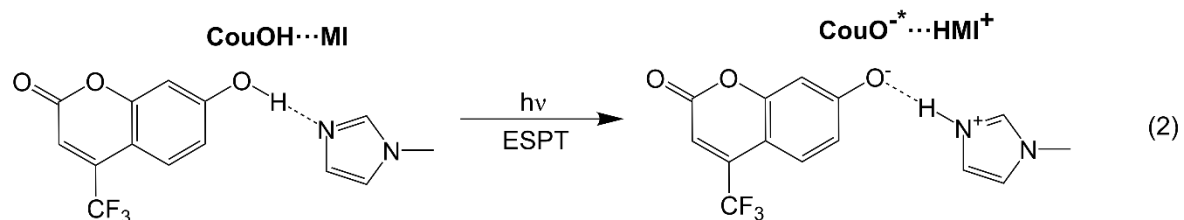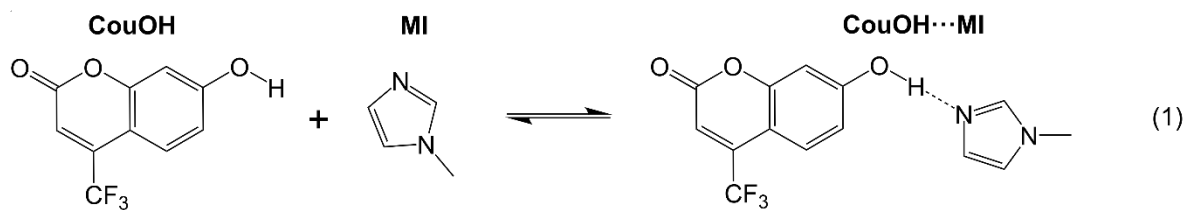
Scheme 1. Reaction schemes for (1) ground state hydrogen-bonding equilibrium between CouOH and MI, (2) excited state proton transfer, (3) subsequent π-stacking of photoproducts to form exciplex.
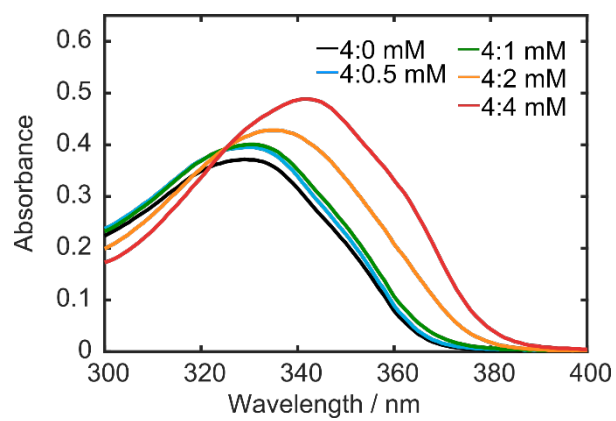
Figure 1. Ultraviolet absorption spectra for the specified CouOH:MI mixtures in deuterated chloroform solution (100 μm pathlength cell).
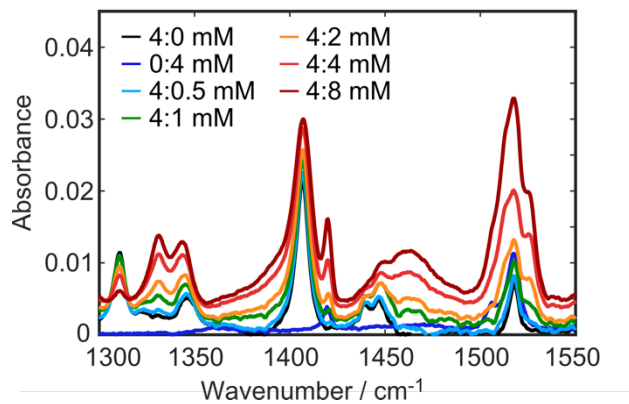
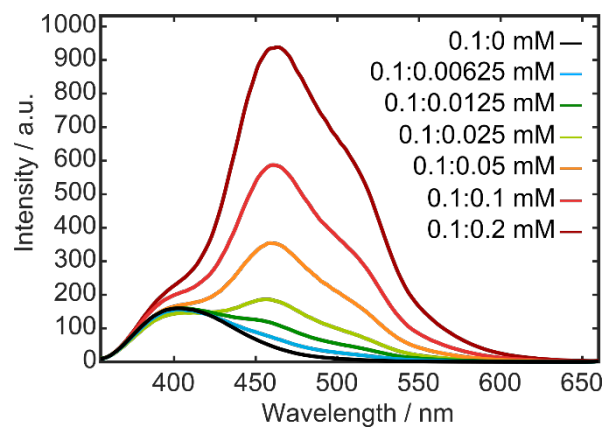**Figure 2.** Ground state mid-IR absorption spectra for the specified CouOH:MI concentrations in CDCl₃.

Figure 3. Fluorescence spectra for the specified CouOH:MI concentrations in CDCl$_3$ using 340 nm excitation.
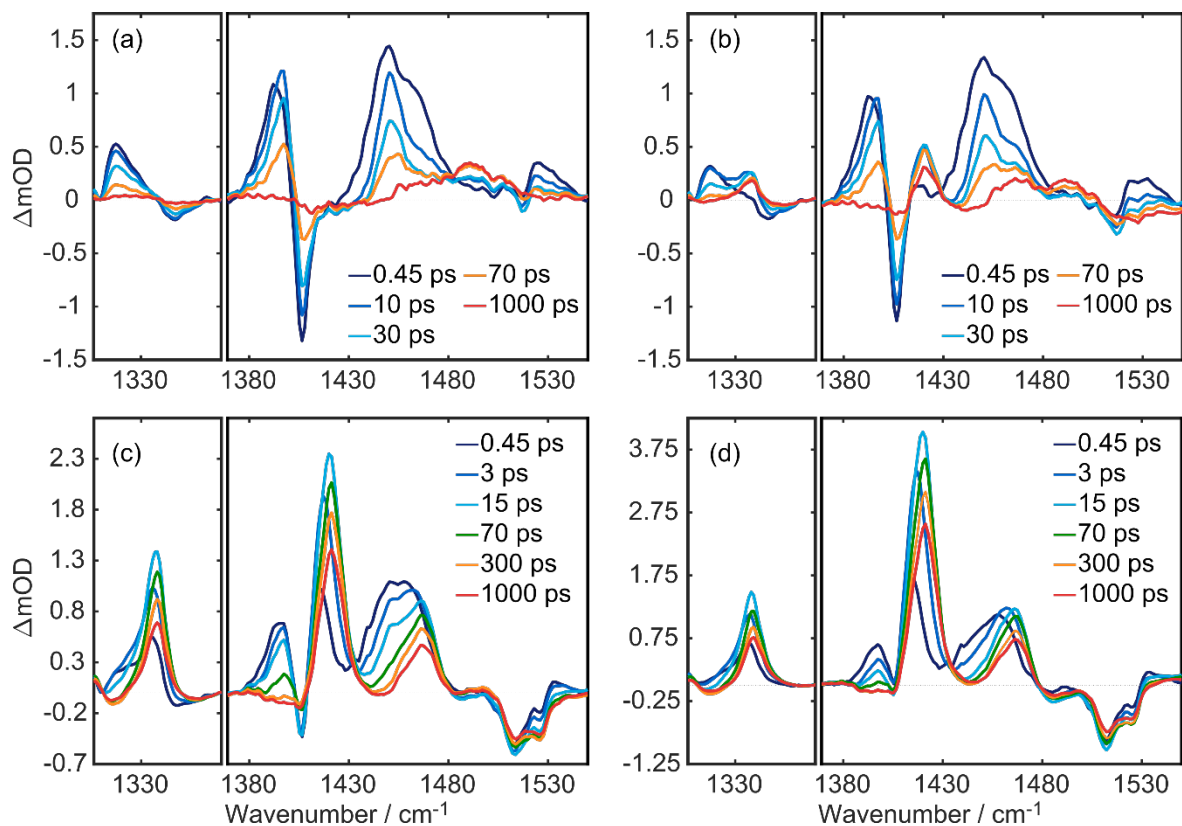
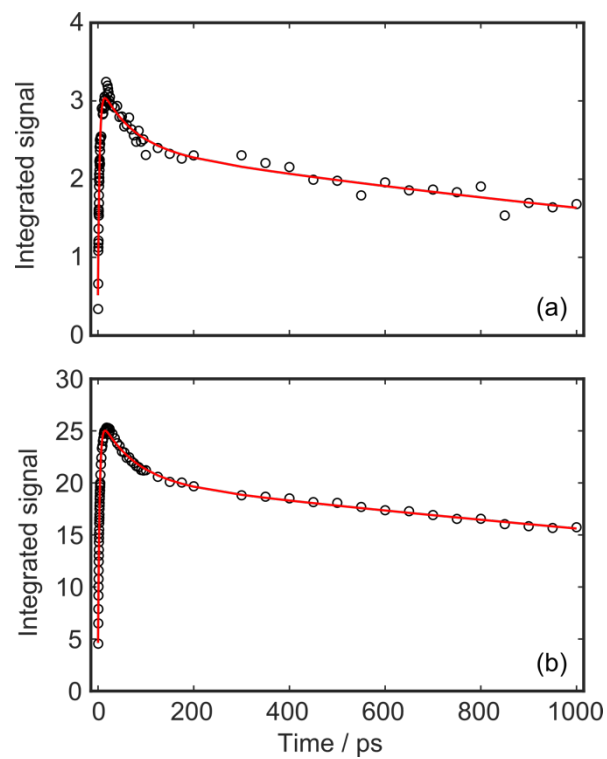**Figure 4.** Transient infrared spectra for (a) CouOH 4 mM, (b) CouOH 4 mM and 1 mM MI, (c) CouOH 4 mM and 4 mM MI, and (d) CouOH 4 mM and 8 mM MI.

Figure 5. Integrated signal for the vibrational band centered at 1420 cm^{-1} (black circles) and tri-exponential fits to data (red line) for (a) 4 mM CouOH and 1 mM MI and (b) 4 mM CouOH and 8 mM MI solutions.
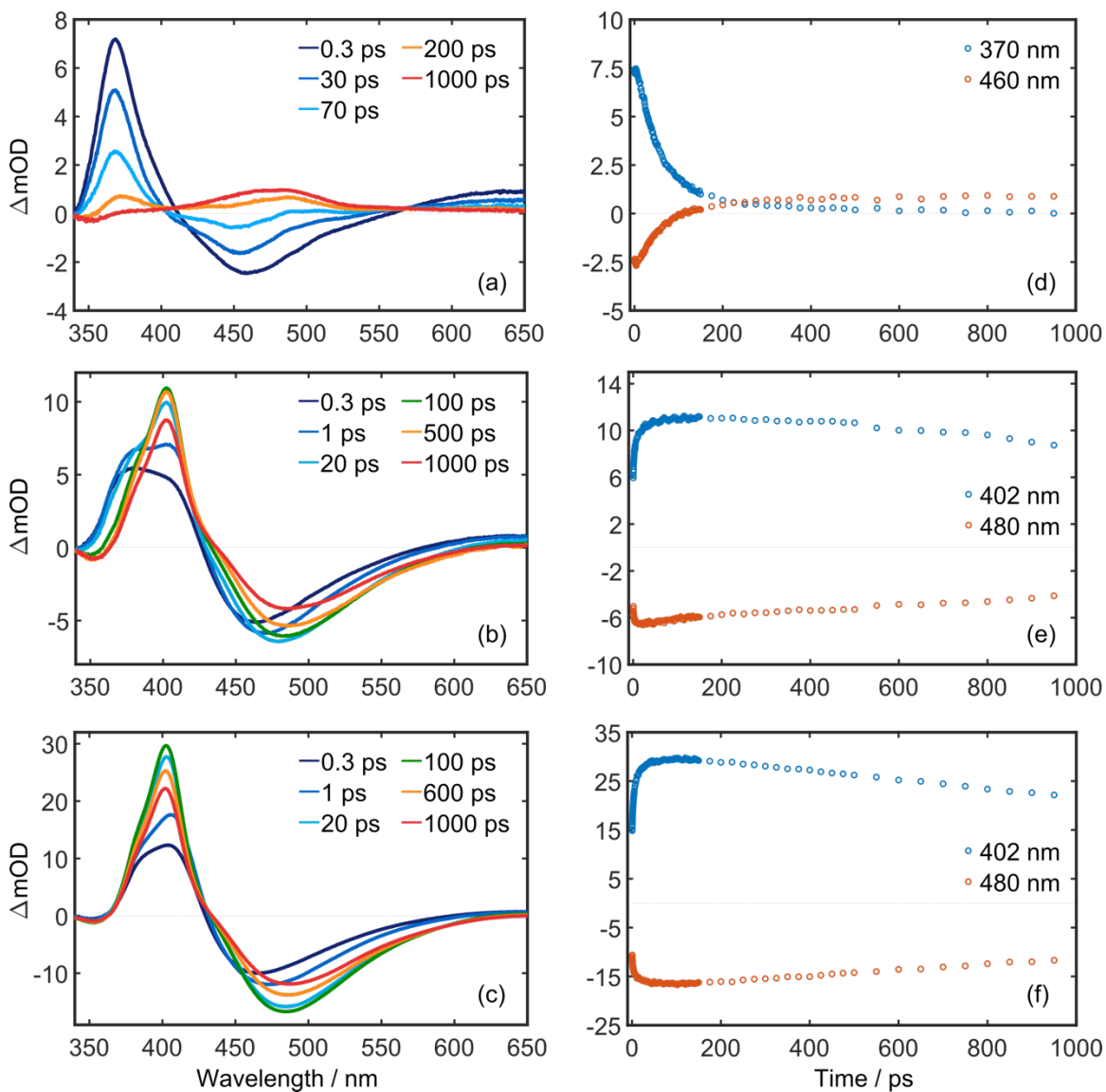
Figure 6. Transient absorption spectra at displayed pump-probe time delays for (a) 4 mM CouOH (b) 4 mM CouOH and 1 mM MI, (c) 4 mM CouOH and 8 mM MI solutions. (d-f) Associated kinetics for displayed probe wavelengths and respective mixtures.
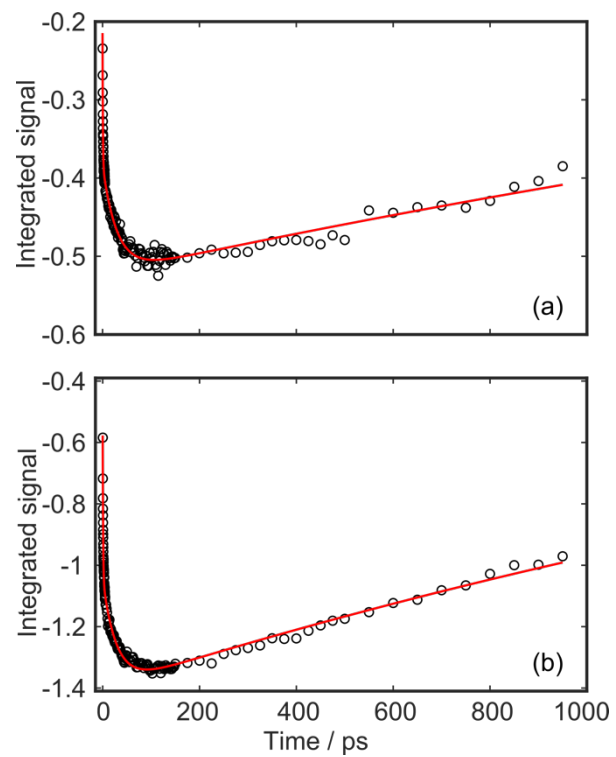
Figure 7. Integrated signal intensity for the stimulated emission centered at 470 nm (black circles) and triexponential fits to data (red line) for (a) 4 mM CouOH and 1 mM MI and (b) 4 mM CouOH and 8 mM MI solutions.
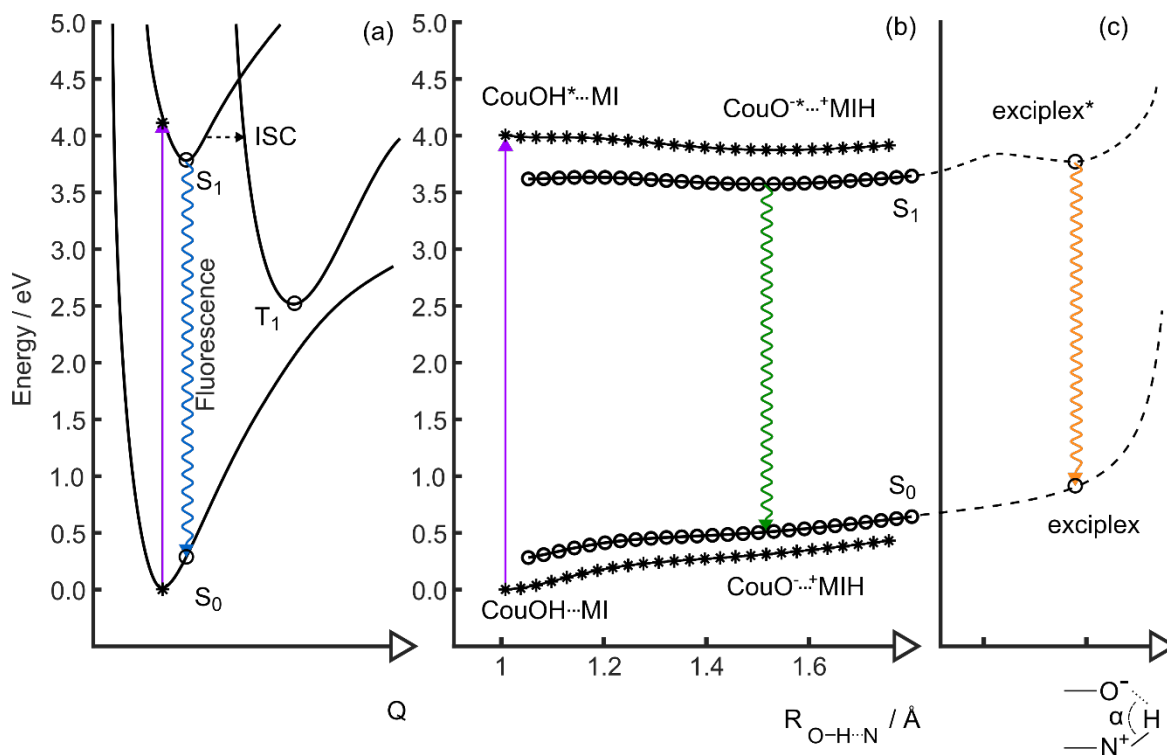
Figure 8. (a) Schematic potential energy surface (PECs) for CouOH based on DFT optimized structures of several key geometries (o symbols). (b) PECs associated with the O–H stretch co-ordinate of CouOH⋯MI. The O–H bond length was held at the displayed values and the rest of the geometry optimized for the S_1 or S_0 states, as denoted by o and ∗ symbols respectively. (c) Schematic PEC based on the exciplex S_1 minimum energy structure, and respective S_0 energy at this geometry as a function of the ∠OHN angle

TOC Graphic

ESPT